Cell Reports
Physical Science

CellPress
OPEN ACCESS

Article

One-step polymer assisted roll-to-roll gravure-printed perovskite solar cells without using anti-solvent bathing

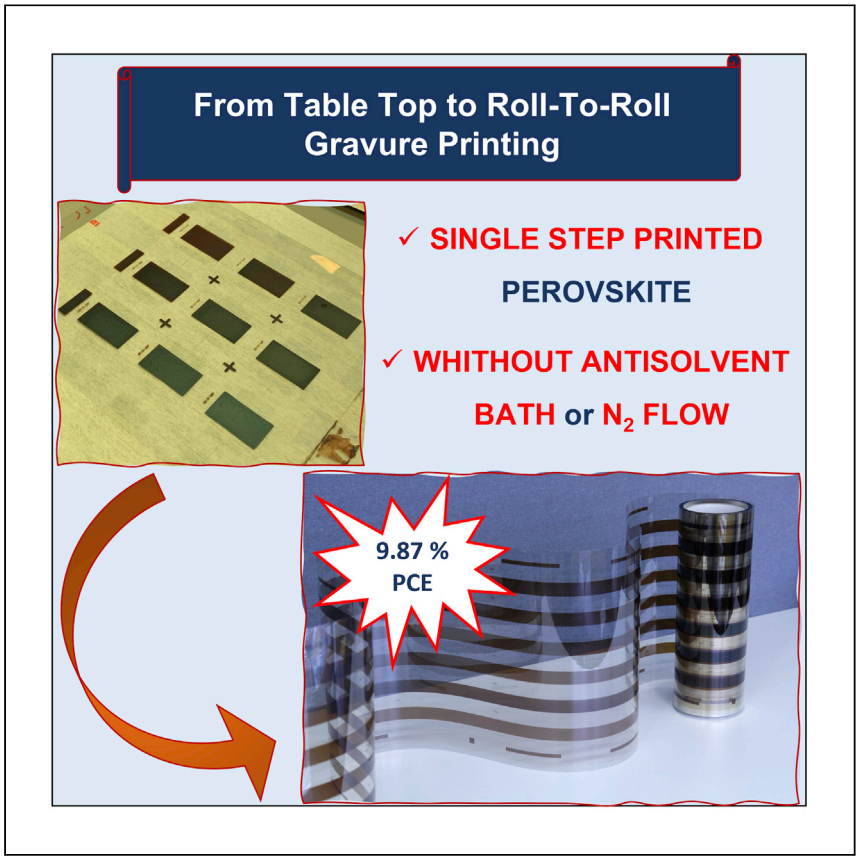

Bisconti et al. take advantage of a starch polymer as a rheological modifier in precursor solutions to deposit perovskite films in one step, avoiding the anti-solvent bath. Roll-to-roll gravure-printed perovskite films and flexible solar cells are demonstrated, reaching a maximum power conversion efficiency close to 10%.

Francesco Bisconti, Antonella Giuri, Riikka Suhonen, ..., Gianluigi Marra, Silvia Colella, Aurora Rizzo

aurora.rizzo@nanotec.cnr.it

Highlights

Viscosity of perovskite-starch inks can be adapted to gravure printing requirements

The viscosities required for gravure are reached with ~50% less of the raw precursors

Polymer endows perovskite with easy processability on a large area without anti-solvent bath

Flexible solar cell fabricated by roll-to-roll processing with maximum PCE of ~10%

Bisconti et al., Cell Reports Physical Science 2, 100639
November 17, 2021
https://doi.org/10.1016/j.xcrp.2021.100639

Cell Reports
Physical Science

CellPress
OPEN ACCESS

Article

One-step polymer assisted roll-to-roll gravure-printed perovskite solar cells without using anti-solvent bathing

Francesco Bisconti,[1,2] Antonella Giuri,[1] Riikka Suhonen,[3] Thomas M. Kraft,[3] Mari Ylikunnari,[3] Ville Holappa,[3] Riccardo Po',[4] Paolo Biagini,[4] Alberto Savoini,[4] Gianluigi Marra,[4] Silvia Colella,[5] and Aurora Rizzo[1,6,*]

SUMMARY

High-throughput manufacturing of hybrid halide perovskite solar cells is the next challenge before they enter the market. An anti-solvent bath is generally required to control the perovskite film assembly starting from precursors in solution. Although an anti-solvent bath has proven feasible for roll-to-roll deposition, it implies an undoubted increased complexity of the manufacturing line, meaning enhanced costs for the process itself and anti-solvent disposal. Here, we take advantage of the use of a starch polymer as a rheological modifier in perovskite precursor solutions to avoid the anti-solvent bath. Starch allows for control of the perovskite growth process in one step and reach of required viscosities for gravure-printing technique with ~50% less of the raw precursor materials. This combined with simplified processing conditions are expected to drastically lower the costs of perovskite material production. We demonstrate that this approach can be upscaled to roll-to-roll gravure printing of flexible solar cells, reaching a maximum power conversion efficiency close to 10%.

INTRODUCTION

Hybrid halide perovskites are proving to be an excellent material for next-generation photovoltaics, demonstrating outstanding power conversion efficiencies over 25% measured in lab-scale devices.[1–3] Nonetheless, perovskite solar cell (PSC) record efficiencies are reached only by an extreme control of environmental conditions (i.e., inert atmosphere and ambient temperature below 25°C[4]), in a narrow window of processing parameters by means of non-scalable techniques (i.e., spin-coating often associated with solvent dripping), and with the use of highly toxic solvents.[5,6] A fine control of the perovskite deposition is mandatory because the film formation occurs throughout a complex self- assembly process driven by weak interactions of perovskite precursor species in solution. Such an intrinsically disordered self-assembly process translates into critical material deposition reproducibility, which hampers a facile upscaling of PSC fabrication.[7–11]

On the lab scale, anti-solvent dripping, performed during perovskite film crystallization from solutions, is exploited to induce a rapid supersaturation of perovskite precursors in the forming film, along with a fast solvent evaporation.[12–14] Such a nucleation-driven formation mechanism results in a perovskite morphology with small grains and highly performing devices. Although integrating antisolvent dripping or bath in the

[1]CNR NANOTEC – Istituto di Nanotecnologia, c/o Campus Ecotekne, Via Monteroni, 73100 Lecce, Italy

[2]Dipartimento di Matematica e Fisica "E. De Giorgi," Università del Salento, Campus Ecotekne, via Arnesano, 73100 Lecce, Italy

[3]Sensing Solutions, VTT Technical Research Centre of Finland Ltd. Kaitoväylä 1, Oulu 90571, Finland

[4]Renewable Energy, Magnetic Fusion and Material Science Research Center, Istituto Guido Donegani, Eni S.p.A., via Fauser 4, I-28100 Novara, Italy

[5]CNR NANOTEC - c/o Dipartimento di Chimica, Università di Bari, Via Orabona 4, 70126 Bari, Italy

[6]Lead contact

*Correspondence: aurora.rizzo@nanotec.cnr.it

https://doi.org/10.1016/j.xcrp.2021.100639

manufacturing line is technically feasible, it increases manufacturing costs. Moreover, the use of extra and generally toxic solvents that need to be disposed of in a large amount should be avoided.[15] Ideally, the manufacturing process has to be as simple as possible and tolerant to variations in the environmental conditions. That being said, there has been significant developments in recent years to bring viability to the large-scale manufacturing of perovskite photovoltaics in roll-to-roll (R2R) facilities.[16–18]

In the attempt to upscale the solvent dripping effect to suit large area R2R manufacturing, various methods have been developed, as follows: anti-solvent dripping or bathing,[4,19] nitrogen blowing,[20] flash infrared annealing,[21] hot substrate,[22] or vacuum-flash-assisted solution processing (VASP).[23] All of these methods have pros and cons, but they all require the use of an extra apparatus, causing an inevitable increase in manufacturing costs. The reproducibility and the narrow processing window required to obtain perovskite films with good optoelectronic quality are other issues to be solved for R2R applications.

Among the scalable perovskite manufacturing techniques, gravure printing is very attractive because it allows high-throughput deposition and high-resolution patterning simultaneously.[18] Recently, fabrication of PSCs by tabletop and R2R gravure printing has been demonstrated by us by means of anti-solvent bathing,[16,24] reaching a champion device for fully R2R gravure-printed solar cells, apart for the electrodes, on a flexible substrate with PCE above 13%.[16]

Here, we develop a convenient one-step gravure printing approach that allows the facile upscaling of perovskite deposition in R2R at mild temperature and ambient air conditions with the use of low toxicity dimethyl sulfoxide (DMSO) as the main solvent. We exploit starch polysaccharide as a rheological modifier to tune the viscosity of perovskite-polymer formulation, which positively influences the formation of perovskite films by single-step coating. The hydroxyl groups on the biopolymer chains establish hydrogen interactions both with organic cations and with the DMSO solvent leading to solution gelation that allows a convenient viscosity modulation.[25] Importantly, starch inclusion enables very viscous inks (~230 mPa s), which is a prerequisite to print a high-resolution pattern by the gravure technique,[16] at a very low perovskite precursor concentration, namely, ~0.75 M for perovskite/starch versus ~2 M for pure perovskite. In view of application, the use of starch as a rheological modifier in perovskite inks is expected to drastically reduce the overall material cost of about 50%. Our approach does not require the use of an anti-solvent, gas blowing, or hot substrate and can be carried out under ambient conditions without any humidity control. This is an undoubtable advantage in the commercialization of PSCs devices because it can drastically reduce the associated manufacturing costs and avoid the disposal of the large amount of solvent waste that has been used for the anti-solvent bath. Here, we demonstrate the R2R gravure printing of flexible solar cell devices by using pilot manufacturing lines by depositing the aforementioned perovskite/starch inks under ambient conditions by a single-step printing method. The partly printed solar cells were fabricated on 50-m-long flexible substrate rolls with promising power conversion efficiencies near 10%, which at the moment represents the best trade-off between simplified processing conditions/costs and device performance.

RESULTS AND DISCUSSION

Table-top gravure-printing of PSCs

To combine the easy processability of the polymer with their templating effects, we select a starch biopolymer that contains free hydroxyl groups on the backbone. As a

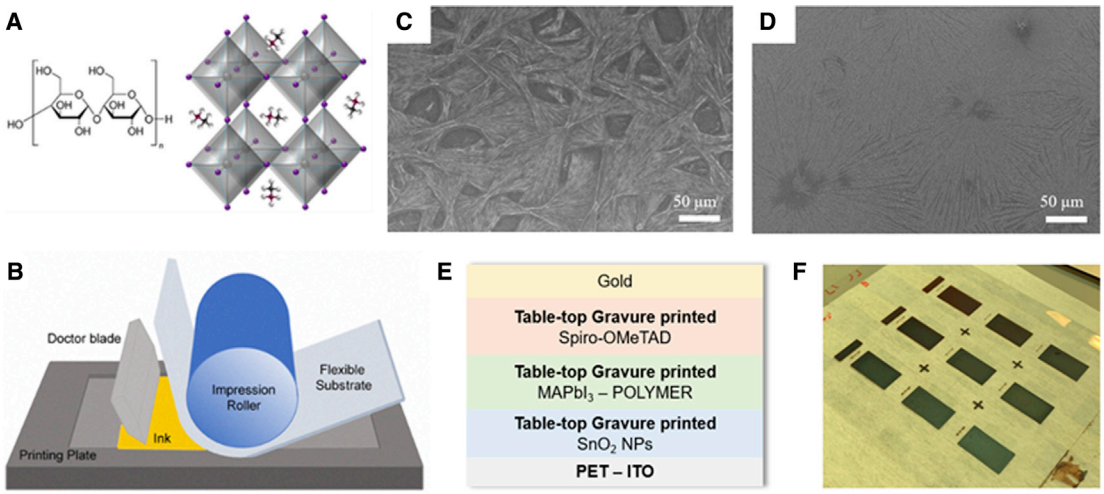

Figure 1. Tabletop gravure-printed perovskite solar cells

(A) Perovskite-starch structures.

(B) Schematic illustration of tabletop gravure printer.

(C and D) Scanning electron microscopy (SEM) images of reference $MAPbI_3$ without anti-solvent (C) and $MAPbI_3$-polymer (30 $MAPbI_3$-10 S, 3:2 DMSO:DMF) printed without anti-solvent bath (D) under ambient conditions. Scale bar, 50 micron.

(E) Sketch of the n-i-p solar cell architecture.

(F) Digital photo of 30 $MAPbI_3$-10 S (perovskite formulation with 30 wt % of perovskite precursors and with 10 wt % of starch), 3:2 DMSO:DMF films deposited by gravure printing.

perovskite material, we focus on the benchmark $CH_3NH_3PbI_3$ ($MAPbI_3$) because it can form a single and stable phase at room temperature.[26] A sketch of the selected materials is reported in Figure 1A.

Previously, we have demonstrated that polycrystalline perovskite films can enormously benefit from the inclusion of starch in terms of mechanical flexibility and processability.[25] In the present work, we take advantage of the use of a starch polymer to guide the formation of perovskite materials in a controlled manner by a gravure printing technique without the use of anti-solvent. Before we printed the composite inks with R2R fabrication at pilot scale, they were tested with a tabletop gravure printer. A schematic drawing of the tabletop gravure printing apparatus is reported in Figure 1B. The ink is deposited on the printing plate with an engraved pattern. Such a printing pattern consists of cells with specific engraving parameters to control the transfer volume of ink, which is doctored to be filled in the engraved patterns. The impression roll's function is to ensure a proper contact of the flexible substrate with the printing plate by external pressure and thus to assist the ink transfer from the cells on the substrate.

The first attempt to deposit pure $MAPbI_3$ perovskite by gravure printing without the use of an anti-solvent bath resulted in a non-uniform film with large aggregate structures and voids. (Figure 1C) This is an expected result because the post-deposition anti-solvent bath was deemed necessary to obtain a suitable perovskite film morphology by the gravure printing technique.[16,24] By adding 10 wt % of starch in the precursor solutions (30 wt % of perovskite precursors), we found that homogenously covered films suitable to solar cells integration were straightforwardly obtained (Figures 1D and 1F). This finding suggests that in our approach, the perovskite crystallization mechanism is completely modified by the polymer inclusion.

Table 1. PV parameters of devices based on different solvent combinations

Perovskite	Jsc (mA/cm2)	Voc (V)	FF (%)	PCE (%)
$MAPbI_3$ reference	Non-working devices			
$MAPbI_3$-starch (9:1 DMSO:DMF)	(20.05 ± 2.13) 21.48	(0.92 ± 0.10) 0.97	(50 ± 8) 56	(9.43 ± 2.81) 11.60
$MAPbI_3$-starch (9:1 DMSO:2-BE)	(20.20 ± 2.22) 22.57	(0.90 ± 0.03) 0.93	(45 ± 6) 50	(8.29 ± 1.88) 10.49
$MAPbI_3$-starch (3:2 DMSO:DMF)	(22.87 ± 0.40) 22.76	(1.02 ± 0.02) 1.00	(47 ± 5) 53	(11.00 ± 1.00) 12.20

Data for average performance were calculated from at least 10 devices. Mean and stardard deviation are given in brackets.

In general, perovskite film formation from solution occurs in four steps, as follows: (1) deposition of perovskite precursors, (2) supersaturation of precursor concentration during solvent removal, (3) formation of crystal nuclei from self-seeding that is induced by supersaturation, and (4) crystal growth starting from formed and complete conversion in crystalline perovskite upon thermal annealing. Because the crystal growth is a fast process, the spontaneous perovskite (without starch additive) assembly leads to the formation of large dendritic structures and inhomogeneous film coverage driven by the imbalance between nucleation and growth rate.[27] A rapid supersaturation and solvent removal are mandatory to reach a high nucleation rate and to obtain a shiny and smooth perovskite layer, ensuring PSCs with high efficiency. To this aim, solvent dripping or bathing enables the sudden removal of solvent, thereby boosting a rapid supersaturation of perovskite precursors in the wet film. In the presence of starch, the hydrogen bond interaction of the free hydroxyl groups on the polymer chain with MA cation and DMSO induces the formation of a sol-gel network that increases the viscosity of the perovskite precursors solution.[8,9,25,28] We have demonstrated that the persistence of such a sol phase during the perovskite film formation actually delays the crystallization process if compared to pure $MAPbI_3$.[28] The precursor solvate phase longevity broadens the deposition time, eventually allowing a single-step coating of perovskite film with uniform coverage, without an anti-solvent bath or dripping, suitable to device integration.[25,29] The retarded crystallization process results in the formation of large perovskite structures, also visible in Figure 1D, and to the formation of more thermodynamically stable perovskite material[28] that could be deposited in an ambient environment.

The developed composite material was tested in a n-i-p solar cell architecture in combination with an SnO_2 electron transporting layer (ETL) and Spiro-OMeTAD hole transporting layer (HTL), by using pre-patterned ITO as the cathode on a flexible PET substrate (Figure 1E). The entire printing process was performed in a controlled temperature (20°C) atmosphere with humidity ranging from 30% to 50%. The sputter coating of indium tin oxide (ITO) on (polyethylene terephthalate) PET and the thermal evaporation of gold as the anode top electrode were the sole non-printing steps. A colloidal dispersion of tin oxide nanoparticles (SnO_2 NPs) in water was printed with the use of 2-propanol as a co-solvent to reduce the surface energy of the solution, obtaining a uniform film without pinholes. Atop of the SnO_2 layer, different formulations of perovskite-starch inks were printed to evaluate different solvents to achieve gravure-printed perovskite film with suitable morphology and crystallinity. The absorption spectra of perovskite-starch films printed starting from inks with a different solvent mixture are reported in Figure S1. The best performance, characterized by a PCE of 12.2%, was obtained by the one-step anti-solvent-bath-free printing of the perovskite-polymer ink based on a mixture of 3:2 DMSO:dimethyl formamide (DMF) as the solvent system (see Table 1).

As it can be readily seen, the as prepared perovskite films look reflective and homogeneous, and by means of a tabletop gravure printing technique, a printed area of

7.5 cm^2 could be reached without sacrificing the homogeneity of the deposited films. With the aim of optimizing device performance, we have tested several solvent combinations; either 2-butoxyethanol (2-BE) or DMF were used as co-solvent together with DMSO to improve the wettability of the substrate, keeping the $MAPbI_3$ concentration (30 wt %) and starch content (10 wt %, related to perovskite precursors) constant. We found that the mixing DMSO and DMF in a 3:2 ratio led to thicker films with more intense absorption (Figure S1) and to the best performing devices, reaching a maximum power conversion efficiency of 12.2% (see Table 1). Morphological and structural analysis were also carried out, and the results are reported in Figure S2 and S3, respectively. The higher short circuit current for the best formulation is due to the higher thickness of the resulting perovskite films and the slightly enhanced open-circuit voltage (V_{OC}) that suggests the formation of sharper interfaces. As expected, devices prepared using gravure-printed pure $MAPbI_3$ did not work due to the poor morphology of the active layer (Figure 1C) likely causing current shorts.

Roll-to-roll printing of PSCs

Here, we prove that our starch perovskite ink deposition can be extended to pilot scale R2R gravure printing manufacturing. The addition of starch indeed confers a suitable viscosity to the perovskite inks to be deposited with a proper thickness. Relevantly, the use of starch allowed an increase of the viscosity of the inks without increasing the concentration of perovskite precursors, reaching a viscosity of ~500 mPa s at a lower shear rate and ~200 mPa s at a higher shear rate. Indeed, it is reported that to enhance the perovskite ink viscosity to make it suitable for R2R gravure (~23.9 mPa s), the perovskite precursor concentration needs to be increased up to 1.69 M,[16] whereas a far higher viscosity (one order of magnitude higher) can be obtained at a perovskite precursor concentration of 0.75 M by using starch as a rheological modifier (Figure S4). Because the cost of starch is marginal in the perovskite ink formulation, our approach effectively reduces the overall material costs of about 50%.

The possibility to produce perovskite inks with high viscosity is also important to achieve perovskite patterns with high resolution.[16] As it can be readily observed, by using starch/perovskite inks, the pattern was reproduced with good precision and the edges were sharp and without a tailing effect. (Figure 2; Figure S5)

The schematic illustration and a photograph of the pilot scale R2R apparatus is reported in Figure 3. To construct the fully printed solar cells, SnO_2 nanoparticles, functioning as ETL, were first printed onto a pre-patterned flexible ITO/PET web and then rapidly annealed. A starch perovskite composite was subsequently printed by R2R gravure without the use of air blowing or anti-solvent bathing, and finally annealed in a hot-air oven, or by adding an infrared (IR) step before the oven, to obtain a desired crystallization. Four rolls were fabricated for the best performing starch perovskite inks (3:2 DMSO:DMF) with different printing speed and annealing parameters, as summarized in Figure 3A. For each roll, an engraving roll with multiple engraved patterns was used (100, 120, and 150 lines/cm). The R2R solar cell stacks were completed with the tabletop printing of poly(3-hexylthiophene) (P3HT) as HTL, which was selected instead of Spiro-OMeTAD because, being a polymer, it features better film-forming properties and printability than Spiro-OMeTAD.[16]

Perovskite starch morphological characterization on the as-prepared 4 rolls is reported in Figures 4 and S6. All the printing parameters resulted in well covered films,

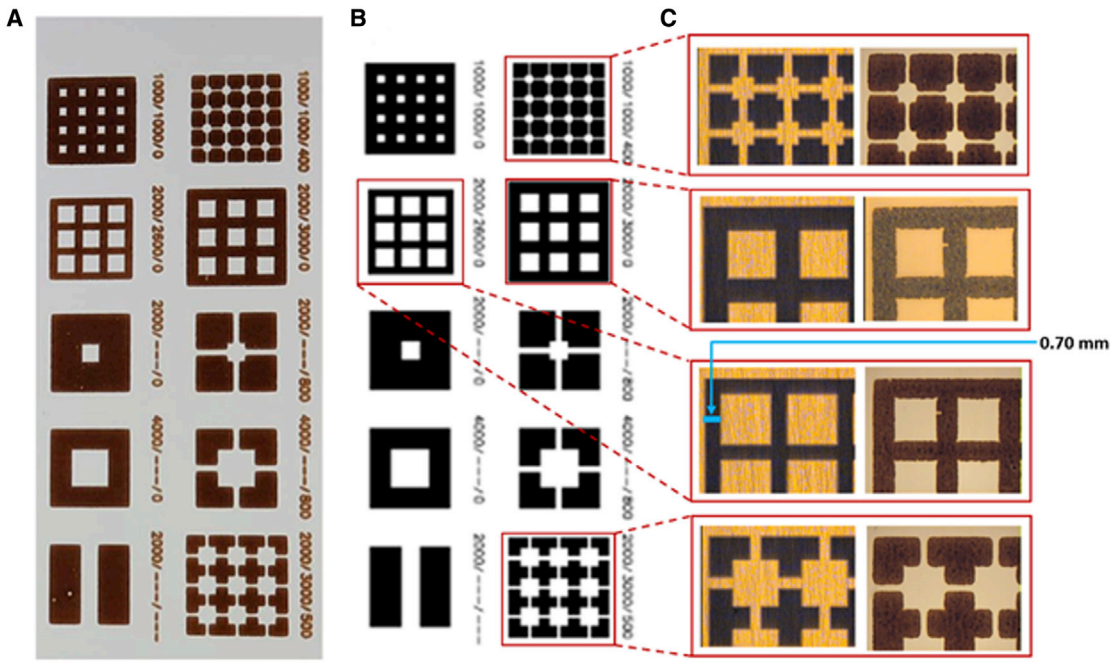

Figure 2. Resolution of the gravure-printed pattern

(A) Digital photos of the printed perovskite-starch ink on PET substrate without anti-solvent bath,reproducing the (B) engraved pattern.

(C) Optical microscope images of the printed perovskite patterns evidencing the good precision. Scale bar for the highlighted pattern is 0.70 mm.

albeit with some differences. The starch-perovskite composite printed at higher speed formed smaller grains, whereas a slower speed formed a big bundle-like structure composed by smaller and cohesive grains. Thus, we confirm that slowing the perovskite formation process results in the formation of more extended morphological structures. We can gather some differences in samples pre-annealed with an IR step. Comparing the morphology of R1 and R2, which were printed at the same speed, we can observe that the IR pre-annealing step induces the formation of more dendritic-like morphology, maybe resulting from a faster annealing process.

Overall, the root means square roughness (Rq) of the starch/perovskite films, extrapolated from the atomic force microscopy (AFM) imaging, is below 40 nm for all the samples thus suitable for device integration.

From the (X-ray diffraction) XRD data (Figure 5A), all the perovskite/starch films showed the characteristic main reflection of $MAPbI_3$ perovskite material at 14.1° and some minor residual contributions from the MAI-PbI_2-DMSO intermediate phase at 6.6°, 7.1°, and 9.2°.[4] Furthermore, we calculated, for each roll, the ratio between the intensity of the signal at 6.6° with that of the main reflection of perovskite (Figure 5B). Interestingly, the results are in accordance with photovoltaic parameters (Figure 6C). R1 indeed showed the best device performance and almost fully converted the perovskite phase, along with a more compact morphology (Figures 4A and 4B).

The solar cell performance for starch/perovskite deposited under different conditions along with photographs of the printed devices (for a total of 50 m) are reported in Figure 6. Solar cells performances tested for all the different engraving parameters are reported in supporting information for completeness (Figures S7). Solar cells with an active area up to 77 mm^2 were also fabricated (Figures S8 and S9).

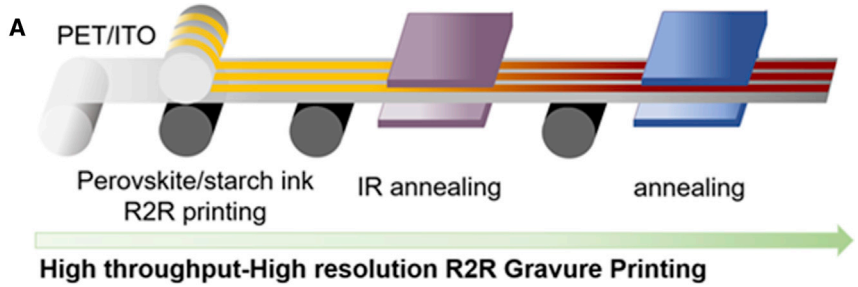

ROLL ID	PEROVSKITE/STARCH PRINTING PARAMETERS	
	Speed (m/min)	Annealing
R1	1.1	3.6 min. at 105 °C
R2		IR + 3.6 min. at 105 °C
R3	3.0	IR + 1.3 min. at 105 °C
R4		IR + 3.6 min. at 105 °C + 2nd annealing

Figure 3. Roll-to-roll printed SnO_2 and perovskite

(A) Sketch of the R2R printing process of the as-developed perovskite/starch inks, along with a table summarizing the processing parameters used for the 4 different rolls.

(B) A photograph of the R2R pilot line.

Relevantly, all the devices fabricated with the 4 rolls worked, corroborating the homogeneity of the deposited perovskite on the 50 m-long PET substrate. The champion device was obtained with roll 1 with a PCE close to 10%, and the maximum power point current (J_{MPP}) measurement is reported in Figure S10. The higher optoelectronic quality of the roll 1 is likely due to a more homogeneous perovskite film morphology and to a better conversion of perovskite, in accordance with the XRD analysis.

The generally limited PCE efficiency is ascribed to low fill factor (FF) values, which can be due to the high sheet resistance of the ITO on PET (50 Ω/sq).[30] A further optimization is needed on the device architecture to obtain solar cells with high efficiency.

In conclusion, we demonstrate that, thanks to the easily tuneable viscosity, such perovskite-starch inks can be adapted to the requirements of gravure printing. We

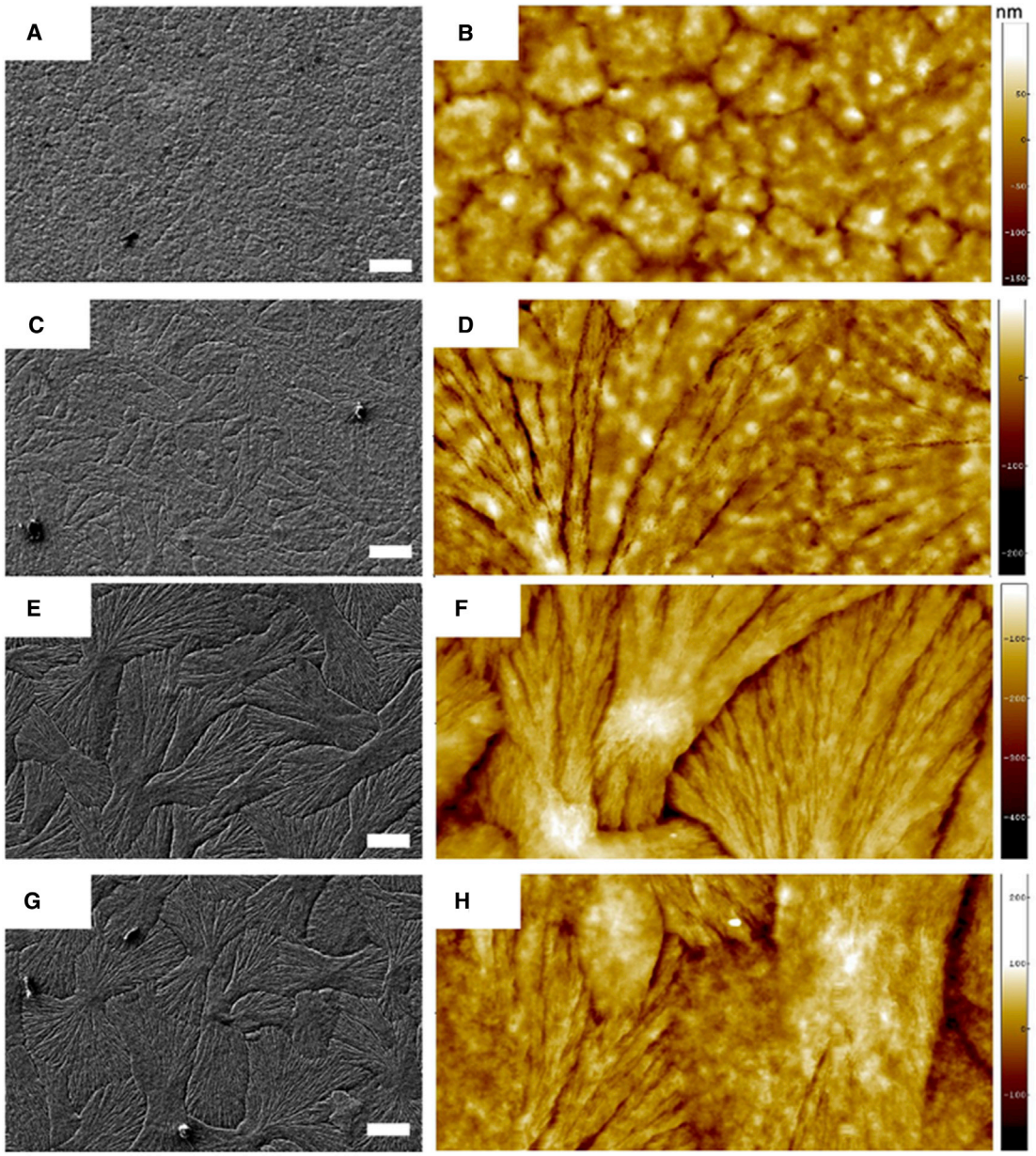

Figure 4. Morphological characterization

SEM (left column) and AFM (right column) of R1 (A and B), R2 (C and D), R3 (E and F), and R4 (G and H). SEM scale bars, 10 μm; AFM x-range; 30 μm.

endow hybrid halide perovskites with the easy processability of polymers, providing a tool to control film formation on a large area by scalable techniques. The superior film-forming properties of polymeric materials guarantees the deposition of perovskite films on large-area flexible substrates without the use of the anti-solvent bath, thus significantly simplifying the large-scale processing that is a mandatory prerequisite in view of the large-scale manufacturing of PSCs at low cost. Importantly, the use of the starch polymeric rheological modifier in the perovskite precursors allows high viscosity to be reached, which is mandatory to obtain a high-resolution pattern by the gravure printing, at less than half of the perovskite precursor concentration. This is expected to reduce the costs for raw materials for PSCs on a large scale of

A

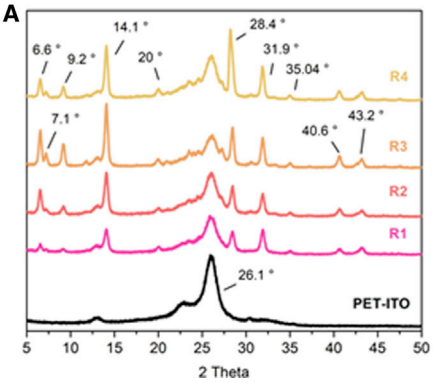

B

	6.6 ° (2θ) (a.u) A	14.1 ° (2θ) (a.u) B	A/B
R1	0.22	1.95	0.11
R2	0.78	1.73	0.45
R3	1.04	4.95	0.21
R4	0.54	2.27	0.24

Figure 5. X-ray diffraction of R2R printed perovskite

(A and B) XRD analysis carried out on the R2R printed perovskite-starch films (A) and calculated ratio between the intensity of the intermediate phase and perovskite signals for each condition of deposition (B).

about 50%. Flexible solar cells fabricated by R2R processing reached a maximum PCE close to 10% that represents the best compromise in terms of process simplification and performance.

EXPERIMENTAL PROCEDURES

Resource availability

Lead contact

For further information on this work, you can communicate with the Lead Contact Aurora Rizzo (aurora.rizzo@nanotec.cnr.it).

Materials availability

This study did not generate new unique materials.

Data and code availability

All experimental data generated from this work are reported in the paper and in the Supplementary Information.

Chemicals

Lead (II) iodide (PbI_2, ultradry 99.999% metals basis) and methylammonium iodide (CH_3NH_3I, MAI) were purchased from Alfa Aesar (Kandel, Germany) and GreatCell Solar (Rome, Italy), respectively. Starch (S); dimethyl sulfoxide anhydrous, 99.9% (DMSO); dimethyl formamide (DMF); chlorobenzene (CB); and 2-butoxyethanol (2-BE) were purchased from Sigma-Aldrich. Tin (IV) oxide NPs (15% in H_2O) were purchased from Alfa Aesar, and $N^2,N^2,N^{2'},N^{2'},N^7,N^7,N^{7'},N^{7'}$-octakis(4-methoxyphenyl)-9,9′-spirobi[9H-fluorene]-2,2′,7,7′-tetramine (Spiro-MeOTAD), lithium bis(trifluoromethanesulfonyl)imide (≥99%, Li-TFSI), and 4-tert-butyl pyridine (98%, tBP) were purchased from Sigma-Aldrich. Poly(3-hexylthiophene-2,5-diyl) (P3HT) was purchased from Rieke Metals. All materials were used as received without any further purification.

$MAPbI_3$-starch inks

The perovskite-polymer inks were prepared in the following two steps: dissolving the perovskite precursors (PbI_2 and MAI, 1:1) in DMSO or in the solvent system DMSO:DMF (9:1, 4:1, and 3:2) at 80°C for 30 min and then adding this solution to the right amount of starch, following a stirring step at 80°C for 3 h. The same concentration of perovskite precursors (30 wt %) and polymer (10 wt %) was retained for all solvent systems. Rheological analysis of the inks was performed at 20°C by using an Anton Paar MCR-301 rheometer

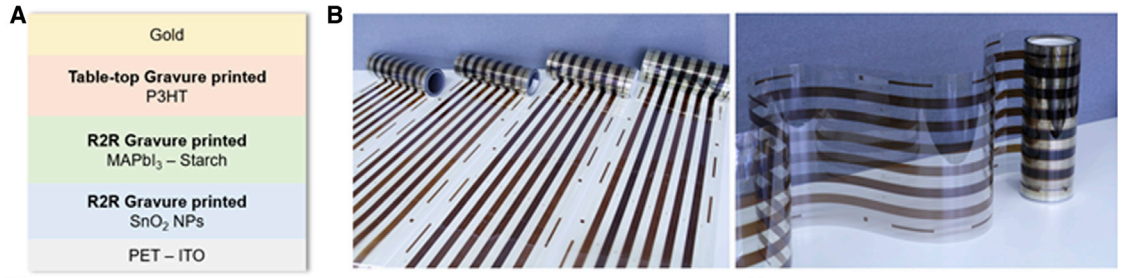

C

Roll ID	Jsc (mA/cm²)	Voc (V)	FF (%)	PCE (%)
Roll 1	16.91 ± 1.53	0.92 ± 0.06	56 ± 11	8.58 ± 1.22
	17.06	**0.89**	**65**	**9.87**
Roll 2	14.79 ± 2.54	0.90 ± 0.06	44 ± 6	5.91 ± 1.67
	16.82	**0.94**	**47**	**7.32**
Roll 3	14.10 ± 3.68	0.85 ± 0.03	56 ± 4	6.68 ± 1.42
	20.97	**0.89**	**49**	**9.22**
Roll 4	17.21 ± 2.33	0.83 ± 0.04	48 ± 8	6.86 ± 1.32
	17.55	**0.88**	**60**	**9.24**

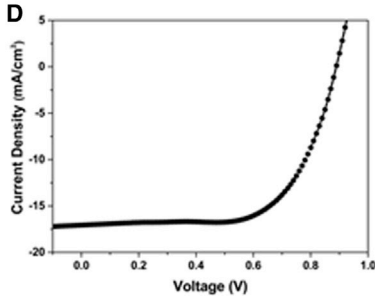

Figure 6. R2R solar cell performances on a flexible substrate

(A) Sketch of the n-i-p solar cell architecture used for the R2R devices.

(B) Digital photos of the 4 rolls deposited by the pilot line R2R gravure printing.

(C) A table summarizing device performances for the four rolls. Best perfomance in bold font.

(D) J-V curve of the champion device obtained with roll 1. At least 24 devices were considered to calculate the average performance.

with cone-plate geometry (1-mm gap). The measurement was conducted in a shear rate range of 2–1,000 1/s, with amplitude sweep at 10 rad/s.

Transporting materials

SnO_2 NPs 15 wt % in water was diluted to 2.5 wt % in H_2O:IPA 50:50. A total of 2.5 mL of a Spiro-MeOTAD solution (85 mg/ml in CB) was doped with 49.9 μl of Li-TFSI (500 mg/ml in acetonitrile) and 82.5 μl of tBP. A total of 4 mL of a P3HT solution (50 mg/ml in CB) was doped with 20 μl of Li-TFSI (500 mg/ml in acetonitrile) and 20 μl of tBP.

Fabrication of tabletop gravure-printed devices

Indium tin oxide patterned polyethylene terephthalate (Estman Flexvue OC50) was used as a flexible substrate, and the desired ITO pattern was realized by rotary screen printing of an etching paste (HiEP-300; P & P Solution Co., Ltd). The ITO/PET roll was cut into 15 × 25 cm^2 sheets for the tabletop printing. A laboratory-scale gravure printer (Labratester, Norbert Schläfli Maschinen) was used in the fume hood. The SnO_2 was printed using a printing plate with an engraved pattern of 120 lines/cm, at a speed of 18 m/min, following an annealing of the SnO_2 in a hot oven at 120°C for 3 min. The $MAPbI_3$ reference and $MAPbI_3$-starch inks were printed using a printing plate with multiple engraved patterns (100, 120, and 140 lines/cm) at a speed of 18 m/min, following an annealing of the resulting films in a hot oven at 100°C for 30 min. The Spiro-MeOTAD layer was printed using a printing plate with an engraved pattern of 100 lines/cm, at a speed of 18 m/min. The device stack was completed by thermal evaporation in high vacuum (5 × 10^{-6} mBar) of 100 nm of gold as the anode with a deposition rate of 1 Å/s and using a mask that defines a 0.06-cm^2 active area.

Roll-to-roll device fabrication

Roll-to-roll gravure printing was conducted by a customized R2R pilot line. A total of 50 m of a PET-ITO roll was used as the substrate, and an Ar/N_2 corona treatment was

performed prior to SnO_2 printing. The ETL ink was printed at a speed of 8 m/min following an annealing step at 120°C for 30 s by a hot air oven. The $MAPbI_3$-starch solution was printed by testing four different printing conditions, as follows: R1 = a speed of 1.1 m/min and 3.6 min of annealing at 105 °C, R2 = a speed of 1.1 m/min and an infrared treatment before a thermal annealing of 3.6 min at 105 °C, R3 = a speed of 3.0 m/min and an infrared treatment before a thermal annealing of 1.3 min at 105 °C, and R4 = a speed of 3.0 m/min and an infrared treatment before a thermal annealing of 3.6 min at 105 °C. Regarding the infrared treatment, two lamps (2 × 500 W) of a drying cassette from Heraeus were used during the R2R processing. An engraving roll with multiple engraved patterns (100, 120, and 150 lines/cm) was used both for SnO_2 and perovskite. After that step, the roll was cut into a single sheet and a P3HT solution was gravure printed by using tabletop setup with a printing plate and an engraved pattern of 100 lines/cm, at a speed of 18 m/min. Finally, 100 nm of gold as the anode was thermally evaporated in high vacuum (5×10^{-6} mBar) with a deposition rate of 1 Å/s and using a mask that defines a 0.06-cm^2 active area.

Perovskite film and device characterization

Morphology of the perovskite-printed samples was analyzed by using scanning electron microscopy with a field emission scanning electron microscope (FE-SEM), Jeol JSM 7600f, with an accelerating voltage of 5 kV. The high-resolution images were collected using a secondary electron signal. AFM characterization was performed with SPM Dimension Icon, Bruker, in the Peak Force Tapping mode in ambient air and at ambient temperature. Digital photos were acquired with an Apple iPhone XR, without any photo manipulation.

X-ray diffraction was conducted by a Panalytical X'Pert alpha-1 Θ/2Θ X-ray diffractometer with gracing incidence geometry with ώ equal to 0.1°, 0.5°, and 1.0° using Cu K_a radiation (l = 1.5416 Å) with the X-ray tube set to 40 V and 40 mA. The spectra were collected in the range 5–90°(2q) with step size 0.02° and time acquisition set to 5 s/step; the qualitative phase analysis of powder samples was carried out by means of the Hanawalt method using the PDF-2 data base (ICDD, International Center of Diffraction Data). The full profile analysis was performed using the Rietveld method implemented in TOPAS software.

Absorption spectra were taken by using an Agilent Cary 5000 UV-VIS-NIR spectrophotometer.

The J-V curves were acquired using a solar simulator (Newport, Oriel Class A, 91195A) with a voltage source meter (Keithley 2420) under 100 mW/cm^2 illumination with standard AM1.5G conditions. Light intensity was calibrated by Si reference cell. The J-V measurements were conducted applying reverse (1.2 V to −0.2 V) and forward (−0.2 V to 1.2 V) scan directions with a voltage step of 0.010 V and a scan rate of 0.5 V/s.

SUPPLEMENTAL INFORMATION

Supplemental information can be found online at https://doi.org/10.1016/j.xcrp.2021.100639.

ACKNOWLEDGMENTS

F.B. gratefully acknowledges the MIUR project "Dottorato Innovativo a Caratterizzazione Industriale (PON R&I 2014-2020)", project code DOT1712250, project

no. 3. The authors gratefully acknowledge Eni S.p.A., Rome, Italy, for the financial support (contract no. 3500047928). A.R. gratefully acknowledges the project Best4U- "Tecnologia per celle solari bifacciali ad alta Efficienza a 4 terminali per utility scale" founded by the Italian Ministry of University ad Scientific Research (MIUR) and Bando PON R&I 2014-2020 e FSC "Avviso per la presentazione di Progetti di Ricerca Industriale e Sviluppo Sperimentale nelle 12 aree di Specializzazione individuate dal PNR 2015-2020"- decreto concessione agevolazione protocollo 991 del 21 maggio 2019 MIUR (contract number PON ARS01_00519 and CUP B88D19000160005). The work is part of the Academy of Finland Flagship Programme, Photonics Research and Innovation (PREIN), decision 320168.

AUTHOR CONTRIBUTIONS

F.B., A.G., S.C., and A.R. conceived the idea. F.B. and R.S. designed the experiments. F.B. and R.S. performed the device fabrication and J-V characterization. R.S. analyzed the solution rheology. F.B., V.H., A.S., and G.M. performed the absorption spectra, XRD, AFM, and SEM analysis. F.B. and A.R. wrote the manuscript. All the authors contributed to the data interpretation, discussion, and manuscript revision.

DECLARATION OF INTERESTS

The authors declare no competing interests.

Received: June 25, 2021
Revised: September 10, 2021
Accepted: October 20, 2021
Published: November 4, 2021

REFERENCES

1. Green, M., Dunlop, E., Kopidakis, N., Hao, X., and Yoshita, M. (2021). Solar cell efficiency tables. Prog. Photovolt. Res. Appl. *29*, 3–15.

2. Jeong, M., Choi, I.W., Go, E.M., Cho, Y., Kim, M., Lee, B., Jeong, S., Jo, Y., Choi, H.W., Lee, J., et al. (2020). Stable perovskite solar cells with efficiency exceeding 24.8% and 0.3-V voltage loss. Science *369*, 1615–1620.

3. Jeong, J., Kim, M., Seo, J., Lu, H., Ahlawat, P., Mishra, A., Yang, Y., Hope, M.A., Eickemeyer, F.T., Kim, M., et al. (2021). Pseudo-halide anion engineering for α-$FAPbI_3$ perovskite solar cells. Nature *592*, 381–385.

4. Jeon, N.J., Noh, J.H., Kim, Y.C., Yang, W.S., Ryu, S., and Seok, S.I. (2014). Solvent engineering for high-performance inorganic-organic hybrid perovskite solar cells. Nat. Mater. *13*, 897–903.

5. Vidal, R., Habisreutinger, S.N., Moore, D.T., Schloemer, T.H., Mora-seró, I., Berry, J.J., and Luther, J.M. (2021). Sustainable solvent selection for the manufacture of methylammonium lead triiodide (MAPbI3) perovskite solar cells. Nat. Sustain. *4*, 227–285.

6. Sánchez, S., Pfeifer, L., Vlachopoulos, N., and Hagfeldt, A. (2021). Rapid hybrid perovskite film crystallization from solution. Chem. Soc. Rev. *50*, 7108–7131.

7. Yan, K., Long, M., Zhang, T., Wei, Z., Chen, H., Yang, S., and Xu, J. (2015). Hybrid halide perovskite solar cell precursors: colloidal chemistry and coordination engineering behind device processing for high efficiency. J. Am. Chem. Soc. *137*, 4460–4468.

8. Masi, S., Rizzo, A., Aiello, F., Balzano, F., Uccello-Barretta, G., Listorti, A., Gigli, G., and Colella, S. (2015). Multiscale morphology design of hybrid halide perovskites through a polymeric template. Nanoscale *7*, 18956–18963.

9. Masi, S., Rizzo, A., Munir, R., Listorti, A., Giuri, A., Esposito Corcione, C., Treat, N.D., Gigli, G., Amassian, A., Stingelin, N., and Colella, S. (2017). Organic Gelators as Growth Control Agents for Stable and Reproducible Hybrid Perovskite-Based Solar Cells. Adv. Energy Mater. *7*, 1602600.

10. Roy, P., Kumar Sinha, N., Tiwari, S., and Khare, A. (2020). A review on perovskite solar cells: Evolution of architecture, fabrication techniques, commercialization issues and status. Sol. Energy *198*, 665.

11. Howard, I.A., Abzieher, T., Hossain, I.M., Eggers, H., Schackmar, F., Ternes, S., Richards, B.S., Lemmer, U., and Paetzold, U.W. (2019). Coated and Printed Perovskites for Photovoltaic Applications. Adv. Mater. *31*, e1806702.

12. Jeon, N.J., Noh, J.H., Kim, Y.C., Yang, W.S., Ryu, S., and Seok, S.I. (2014). Solvent engineering for high-performance inorganic-organic hybrid perovskite solar cells. Nat. Mater. *13*, 897–903.

13. Konstantakou, M., Perganti, D., Falaras, P., and Stergiopoulos, T. (2017). Anti-Solvent Crystallization Strategies for Highly Efficient Perovskite Solar Cells. Crystals (Basel) *7*, 291.

14. Li, J., Yang, R., Que, L., Wang, Y., Wang, F., Wu, J., and Li, S. (2019). Optimization of anti-solvent engineering toward high performance perovskite solar cells. J. Mater. Res. *34*, 2416.

15. Swartwout, R., Patidir, R., Belliveau, E., Dou, B., Beynon, D., Greenwood, P., Moody, N., DeQuilettes, D.W., Bawendi, M., Watson, T.M., and Bulovic, V. (2020). Predicting Low Toxicity and Scalable Solvent Systems for High Speed Roll-to-Roll Perovskite Manufacturing. ChemRxiv. https://doi.org/10.26434/chemrxiv.13221851.v2.

16. Kim, Y.Y., Yang, T.Y., Suhonen, R., Kemppainen, A., Hwang, K., Jeon, N.J., and Seo, J. (2020). Roll-to-roll gravure-printed flexible perovskite solar cells using eco-friendly antisolvent bathing with wide processing window. Nat. Commun. *11*, 5146.

17. Gusain, A., Thankappan, A., and Thomas, S. (2020). Roll-to-roll printing of polymer and perovskite solar cells: compatible materials and processes. J. Mater. Sci. *55*, 13490.

18. Gertsen, A.S., Castro, M.F., Søndergaard, R.R., and Andreasen, J.W. (2020). Scalable fabrication of organic solar cells based on non-fullerene acceptors. Flex. Print. Electron *5*, 014004.

19. Zhou, Y., Yang, M., Wu, W., Vasiliev, A.L., Zhu, K., and Padture, N.P. (2015). Room-temperature crystallization of hybrid-perovskite thin films via solvent–solvent extraction for high-performance solar cells. J. Mater. Chem. A Mater. Energy Sustain. *3*, 8178.

20. Ng, A., Ren, Z., Hu, H., Fong, P.W.K., Shen, Q., Cheung, S.H., Qin, P., Lee, J.W., Djurišić, A.B., So, S.K., et al. (2018). A Cryogenic Process for Antisolvent-Free High-Performance Perovskite Solar Cells. Adv. Mater. *30*, e1804402.

21. Sanchez, S., Hua, X., Phung, N., Steiner, U., and Abate, A. (2018). Flash Infrared Annealing for Antisolvent-Free Highly Efficient Perovskite Solar Cells. Adv. Energy Mater. *8*, 1702915.

22. Nie, W., Tsai, H., Asadpour, R., Blancon, J.C., Neukirch, A.J., Gupta, G., Crochet, J.J., Chhowalla, M., Tretiak, S., Alam, M.A., et al. (2015). Solar cells. High-efficiency solution-processed perovskite solar cells with millimeter-scale grains. Science *347*, 522–525.

23. Li, X., Bi, D., Yi, C., Décoppet, J.D., Luo, J., Zakeeruddin, S.M., Hagfeldt, A., and Grätzel, M. (2016). A vacuum flash-assisted solution process for high-efficiency large-area perovskite solar cells. Science *353*, 58–62.

24. Kim, Y.Y., Yang, T.Y., Suhonen, R., Välimäki, M., Maaninen, T., Kemppainen, A., Jeon, N.J., and Seo, J. (2019). Gravure-Printed Flexible Perovskite Solar Cells: Toward Roll-to-Roll Manufacturing. Adv. Sci. (Weinh.) *6*, 1802094.

25. Giuri, A., Masi, S., Listorti, A., Gigli, G., Colella, S., Esposito Corcione, C., and Rizzo, A. (2018). Polymeric rheology modifier allows single-step coating of perovskite ink for highly efficient and stable solar cells. Nano Energy *54*, 400.

26. Jacobsson, T.J., Schwan, L.J., Ottosson, M., Hagfeldt, A., and Edvinsson, T. (2015). Determination of Thermal Expansion Coefficients and Locating the Temperature-Induced Phase Transition in Methylammonium Lead Perovskites Using X-ray Diffraction. Inorg. Chem. *54*, 10678–10685.

27. Liu, C., Cheng, Y.B., and Ge, Z. (2020). Understanding of perovskite crystal growth and film formation in scalable deposition processes. Chem. Soc. Rev. *49*, 1653–1687.

28. Giuri, A., Munir, R., Listorti, A., Esposito Corcione, C., Gigli, G., Rizzo, A., Amassian, A., and Colella, S. (2021). Implication of polymeric template agent on the formation process of hybrid halide perovskite films. Nanotechnology *32*, 265707.

29. Giuri, A., Yuan, Z., Miao, Y., Wang, J., Gao, F., Sestu, N., Saba, M., Bongiovanni, G., Colella, S., Esposito Corcione, C., et al. (2018). Ultra-Bright Near-Infrared Perovskite Light-Emitting Diodes with Reduced Efficiency Roll-off. Sci. Rep. *8*, 15496.

30. Schmidt, T.M., Larsen-olsen, T.T., Carlé, J.E., Angmo, D., and Krebs, F.C. (2015). Upscaling of Perovskite Solar Cells: Fully Ambient Roll Processing of Flexible Perovskite Solar Cells with Printed Back Electrodes. Adv. Eng. Mater. *5*, 1500569.